Iranian Journal of Science & Technology, Transaction B: Engineering, Vol. 34, No. B1, pp 49-62
Printed in The Islamic Republic of Iran, 2010

DUCTILITY EFFECTS ON THE BEHAVIOUR OF STEEL STRUCTURES UNDER BLAST LOADING*

R. A. IZADIFARD[1**] AND M. R. MAHERI[2]

[1]PhD candidate, Shiraz University, I. R. of Iran
[2]Dept. of Civil Eng., Shiraz University, I. R. of Iran, Email: maheri@shirazu.ac.ir

Abstract– The importance of ductility in absorbing energy and its improving the structural behaviour under earthquake loading is well-established. Some researchers have noted that the ductility ratio may also be an important parameter for designing structures against explosion-induced forces. However, their works were mainly qualitative and based on the ductility of the structural members. In this article, nine short steel frames with different spans and numbers of storeys, subjected to different blast loadings have been investigated. Nonlinear pushover blast force-displacement curves are evaluated for each frame and the ductility parameters are extracted. The results indicate the significant effects of ductility ratio on the structural response. Also, it is found that the ductility reduction factor under blast loading increases with increasing ductility ratio, irrespective of the period of vibration of the system.

Keywords– Ductility ratio, ductility reduction factor, blast loading, steel structures

1. INTRODUCTION

Nowadays, the danger of explosion damage to a structure as a result of a hostile act is on the rise. Many factors can decrease, or increase the detrimental effects of an explosion. The role of ductility in absorbing the energy and modifying the structural behaviour under the effect of earthquake loading is well established. Many researchers have attempted to generalize the loading to include the blast loading.

Smith and Heathernigton reported that field tests have proved that structures with lesser ductility are more susceptible to explosion forces [1]. Based on observations, Smilowitz also believes that ductility of the steel tube system was the major factor in decreasing the effects of destruction in the explosion that happened in the World Trade Center in New York in 1994 [2]. Thabet and Haldane investigated the non-linear behaviour of a 3-D reinforced concrete frame under blast loading by determining its patterns of failure and the effects of ductility on the response [3]. Mendis and Ngo also investigated the susceptibility of tall reinforced concrete structures to blast loading initiated from outside the building and found that in order to avoid progressive collapse, the ductility of members is much more vital than their overall strength [4]. Hinman has also noted that working with ductile materials and designing ductile connections are essential for the safety of structures against blast loading [5]. Khaloo and Tariverdilu Asl also reported on the effects of ductility on the high strength concrete RC flexural members [6]. Regarding other structures, Son et-al. [7] and Runter et-al. [8] assessed the effects of ductility on controlling cracks in bridge decks and piers, both having a positive view on ductility to prevent progressive collapse.

Regarding the general effects of blast loading on structural elements, the results of many investigations are reported in the technical literature. For example, Lussicni and Luege [9] and Miyamoto and Nakamura [10] investigated the effects on reinforced concrete slabs, Lan et-al. [11] as well as.

*Received by the editors January 28, 2009; Accepted December 3, 2009.
**Corresponding author

Librescu et al. [12] studied the effects of blast loading on sandwich paneling, Louca and Boh worked on design and analysis of blast walls [13] and Magnusson and Hallgre carried out blast analysis of reinforced concrete beams [14].

A look at the current state-of-the-art, as indicated above, shows that the previous investigations on ductility effects under blast loading are mostly limited to the materials or the structural elements and in regards to the ductility effects on the structural response as a whole, mainly the results from other dynamic loading such as earthquake loading are adapted for blast loading. Also, the latter research is limited to qualitative investigations and no quantitative work has been carried out. As a result, in this article attention is focused on ductility and its effects on the behaviour of steel frames, built on the ground, under blast loading.

2. DUCTILITY RATIO OF THE STEEL FRAMES

In a dynamic loading, because the load is temporary and its duration is short, it is preferable that materials and connections behave in a non-elastic manner so that the structure can tolerate larger deformations and can absorb more energy. The ratio of the ultimate displacement to displacement at the point of yield is called ductility ratio [15].

In Fig. 1a, the displacement-force curve for a steel member is shown. In this diagram, Δ_y is the displacement at the yield point and Δ_u is the ultimate displacement at the point of failure. The ductility ratio (μ) for a steel member is therefore identified as;

$$\mu = \Delta_u / \Delta_y \tag{1}$$

Figure 1b shows the displacement-force diagram for a steel frame. δ_y shows the displacement where the curve changes from a linear form to a non-linear form and represents formation of the first plastic hinge in the frame. On increased loading, through redistribution of internal forces, the stress in other sections will increase and further plastic hinges are developed up to the point where the structure becomes unstable. Δ_y is the crossing point of extension of the elastic branch of the curve with asymptote of the final point of force-displacement curve. Δ_y is considered as the virtual or effective structural yield point. Δ_u corresponds to the displacement at which the frame reaches its ultimate capacity. However, to avoid destruction of the structure due to the effects of P-Δ, standard codes of practice limit this displacement to a percentage of the height of the structure.

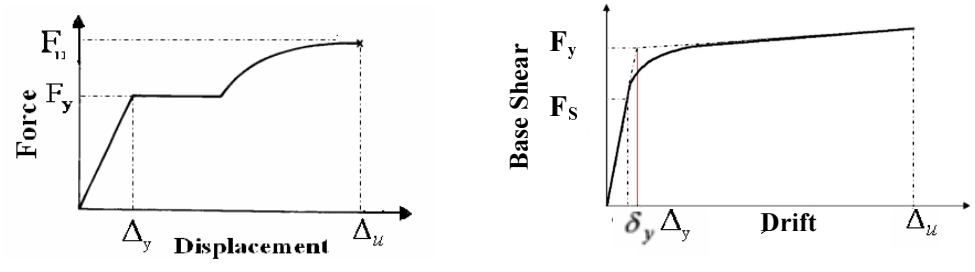

(a) (b)

Fig. 1. Displacement-force diagram for: a) steel bar b) steel frame

In this article, three types of frames are investigated; one span-one storey frames, three span-two storey frames and five span-two storey frames. Each type of frame consists of three frames with different member configurations and properties, giving them different ductility ratios.

Figure 2 represents the geometric specifications and cross-sections of the frame members. The frames are modeled using thin walled elements of the ANSYS software [16], having the capacity to undergo

tension, compression, bending, and St. Venant torsion. The steel is assumed to have an elasto-plastic behaviour with: $E = 200\,GPa$, $v = 0.3$ and $F_y = 240\,MPa$. To calculate the ductility ratio, displacement-controlled, non-linear pushover analysis of the frames were carried out. For this purpose, the ultimate allowable drift was considered to be equal to 2.5% of the height of the structure on the basis of the specification by the Iranian seismic code, standard 2800 [17]. Displacements of up to 2.5% the height of each frame were therefore statically applied at 0.001m intervals and the corresponding frame base shears were calculated. Figure 3 shows the base shear-drift diagrams for the one span-one storey frames (U). In the initial stage, as expected, the change in the base shear in relation to the drift is linear. However, as the drift increases and with the increase in the member stresses, the first and the subsequent plastic hinges occur and as a result the slope of the drift-base shear curve reduces.

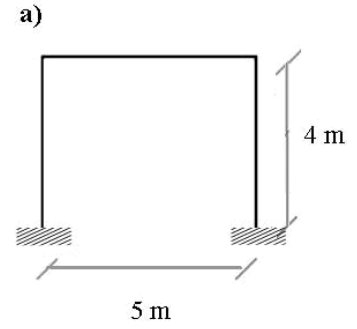

	FRAME		
	U1	U2	U3
Columns	IPB240	IPB300	IPB320
Beam	IPE300	IPE300	IPE300

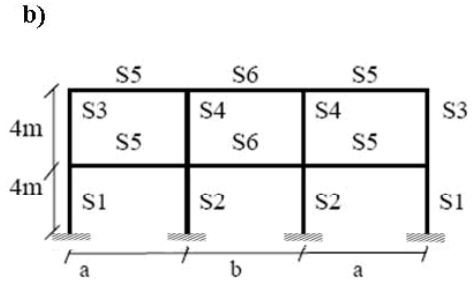

	3F1	3F2	3F3
a	5m	4.25m	4.25m
b	5m	6.5m	6.5m
S1	IPB220	IPB220	IPB280
S2	IPB280	IPB280	IPB320
S3	IPB200	IPB200	IPB260
S4	IPB240	IPB240	IPB280
S5	IPE450	IPE400	IPE360
S6	IPE450	IPE500	IPE500

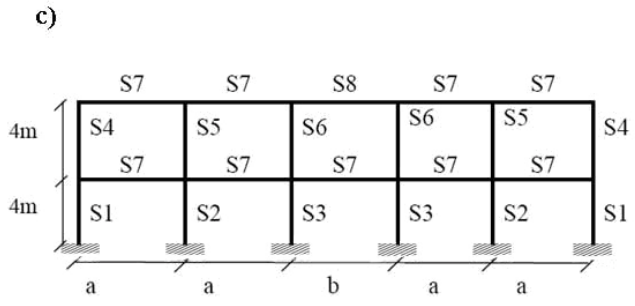

	5F1	5F2	5F3
a	5m	4. 5m	4. 5m
b	5m	7m	7m
S1	IPB220	IPB200	IPB280
S2	IPB240	IPB240	IPB320
S3	IPB280	IPB280	IPB320
S4	IPB200	IPB200	IPB260
S5	IPB220	IPB220	IPB300
S6	IPB220	IPB260	IPB300
S7	IPE450	IPE360	IPE360
S8	IPE400	IPE550	IPE550

Fig. 2. Characteristics of the nine analyzed frames: a) one span-one storey frames, b) three span-two storey frames and c) five span-two storey frames

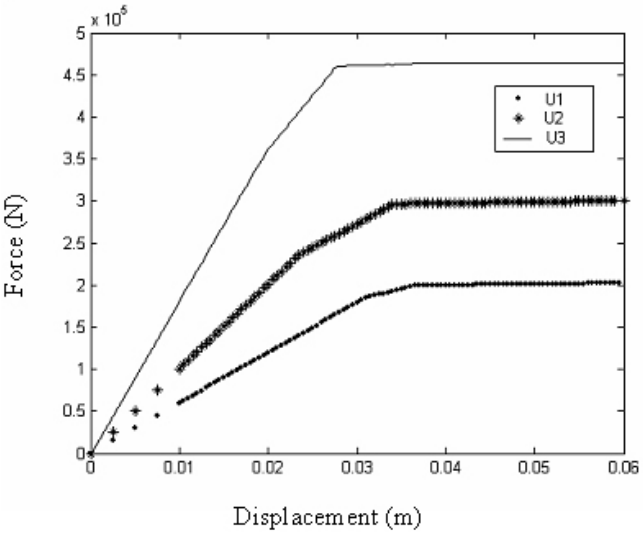

Fig. 3. Force-Roof displacement curve for U_1, U_2 and U_3

The effective structural yield displacements (Δ_y) and the ductility ratios determined for U frames are given in Table 1. Similarly, the ductility ratios for the two-storey frames (3F and 5F) were evaluated and are presented in Table 2.

Table 1. Ductility ratios for the one span-one storey frames

	FRAME		
	U1	U2	U3
Δ_y	0.0334	0.0293	0.0266
Δ_u	0.1	0.1	0.1
Δ_u / Δ_y	3	3.4	3.8

Table 2. Ductility ratio for 3 and 5 span-two storey frames

	FRAME					
	3F1	3F2	3F3	5F1	5F2	5F3
Δu	0.2	0.2	0.2	0.2	0.2	0.2
Δy	0.06	0.054	0.043	0.06	0.053	0.043
$\mu = \Delta u / \Delta y$	3.3	3.7	4.3	3.3	3.8	4.7

3. BLAST LOADING

In this article we have assumed that the blast takes place at a distance outside the structure in a manner in which the whole structure is affected by the blast waves. Also, it is assumed that the explosive charge is positioned on the ground (Fig. 4).

The first step for estimation of loads exerted on the structure by the air blast is to calculate the maximum overpressure. Although different equations for calculation of these parameters have been suggested, the equation by Kinney and Graham [18], and TM5-1300 diagram [19] more accurately estimate this parameter [20]. On the basis of numerical analysis and using experimental data, Kinney and Graham have suggested Eq. (2) for calculation of the maximum overpressure (P_s) [18].

$$\frac{P_s}{P_0}=\frac{808\left[1+\left(\frac{z}{4.5}\right)^2\right]}{\left[1+\left(\frac{Z}{0.048}\right)^2\right]^{\frac{1}{2}}.\left[1+\left(\frac{Z}{0.32}\right)^2\right]^{\frac{1}{2}}\left[1+\left(\frac{Z}{1.35}\right)^2\right]^{\frac{1}{2}}} \tag{2}$$

In this equation, P_0 is the ambient atmospheric pressure, and Z is the scaled distance in $m/kg^{1/3}$ as given in Eq. (3).

$$Z = R/W^{\frac{1}{3}} \tag{3}$$

Where, W is the weight equivalent TNT charge in kg, and R is the distance from detonation point to the point of registered pressure. The velocity of the blast wave propagation in the air (U_s) may be evaluated as [21]:

$$U_s=\sqrt{\frac{6P_s+7P_0}{7P_0}}a_0 \tag{4}$$

In Eq. (4), a_o is the sound velocity in air. The blast wave propagation in the air produces dynamic pressure, which is calculated from Eq. (5) [21].

$$q_s=\frac{5P_s^2}{2(P_s+P_0)} \tag{5}$$

As the blast waves collide with a perpendicular surface, reflection pressure is generated which can be evaluated using the following equation [21];

$$P_r=2P_s\left[\frac{7P_0+4P_s}{7P_0+P_s}\right] \tag{6}$$

To calculate the duration of the blast loading on a structure (t_s), we can use either the diagram presented in TM5-1300 [19] or the Eq. (7) suggested by Izadifard and Maheri [22] as;

$$\begin{aligned}\log_{10}\left(t_s/W^{1/3}\right)&=2.5\log_{10}(Z)+0.28 \quad ; \quad Z\le 1\\ \log_{10}\left(t_s/W^{1/3}\right)&=0.31\log_{10}(Z)+0.28 \quad ; \quad Z\ge 1\end{aligned} \tag{7}$$

First, the blast wave collides with the front face of the structure and causes an intense reflected pressure in the air outside the structure. Then, the wave passes over the structure and reaches the rear of the structure (Fig. 4). The traveling time of the wave from one point to another is proportional to the distribution of the wave in the ambient atmosphere [1]. The on-side pressures, including the suction caused by the drag, are applied on the roof and the rear part of the structure. The drag coefficients on different surfaces are presented in references [1], [19] and [21]. As an example, the pressure exerted on the surfaces of the frame (U) under an explosion of l000 kg of TNT at 30 meters away from the frame is presented in Fig. 5. Also, Fig. 6 shows the exerted pressure on different surfaces of the two-storey frames with three spans (3F) under an air blast of l000 kg of TNT at a distance of 30 meters. As another example, the exerted pressures on different surfaces of the two-storey frames with five spans (5F) under a 4000 kg of TNT blast at a

distance of 50 meters are also shown in Fig. 7. It should be noted that in all the above mentioned analyses, the explosive charge was positioned on the ground and the reflecting effects of the ground are also considered in the calculation.

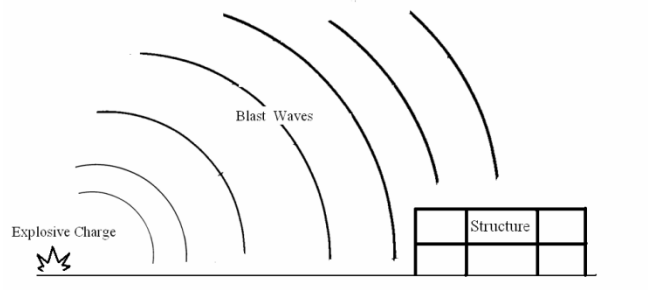

Fig. 4. Blast wave propagation

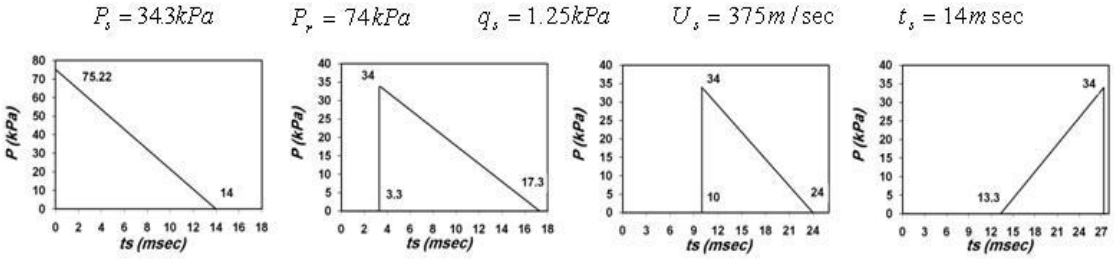

(a) (b) (c) (d)

Fig. 5. Blast loading on U frames; a) near side, b) roof (left side), c) roof (right side), d) far side

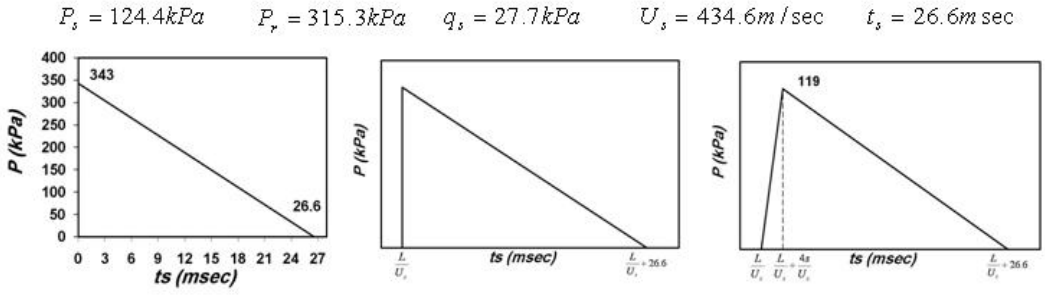

(a) (b) (c)

Fig. 6. Blast loading on 3F frames; a) near side, b) roof, c) far side

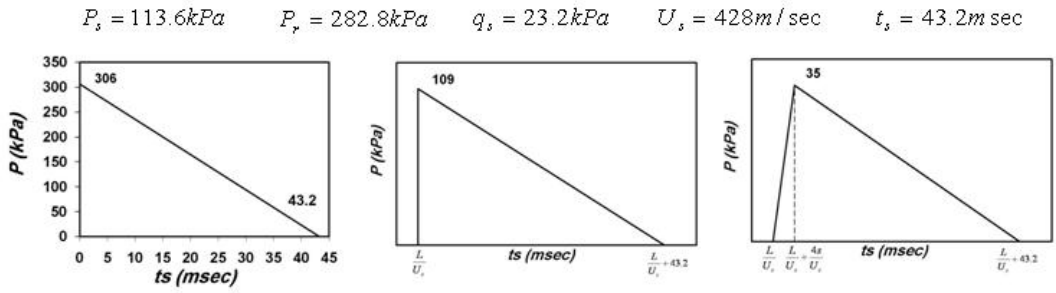

(a) (b) (c)

Fig. 7. Blast loading on 5F frames; a) near side, b) roof, c) far side

4. RESPONSE OF THE FRAMES TO BLAST LOADING

In many dynamic loadings similar to earthquake, the ductility reduction factor, R_μ, is calculated in the following form

$$R_\mu = F_e / F_y \tag{8}$$

where, with reference to Fig. 8, F_e is the ultimate base shear in the linear elastic behavior and F_y is the ultimate base shear in the non-linear elasto-plastic response.

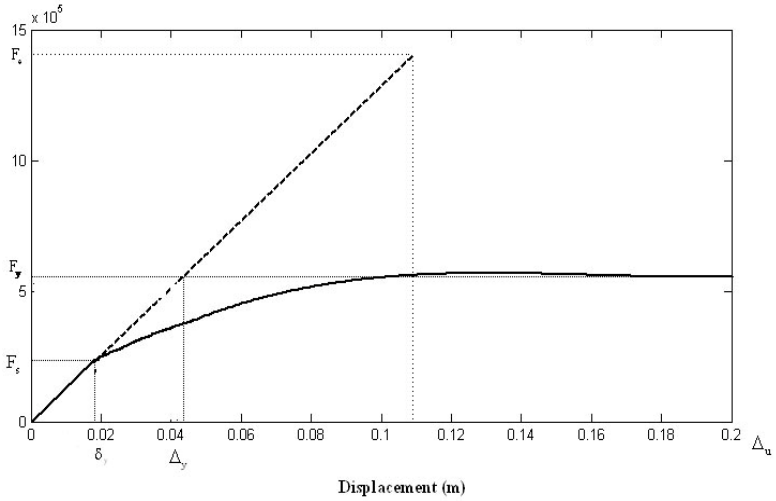

Fig. 8. Roof displacement-base shear for U_1 frame

To determine the ductility reduction factor for the nine frames under blast loading, therefore, the base shear-drift relationship for each frame needs to be established. The following procedure was adopted to evaluate these relationships;

i) For each frame, the blast pressure time history exerted on the near and far sides and the roof of the frame were evaluated as described above, using different payloads exploding at a specified distance away from the frame. Payloads of 5, 10, 20, 30, 40, 55, 70, 85, 100, 115, 130, 150, 175, 200, 225 kg TNT at a distance of 30m were considered for the single storey U frames, with U_2 and U_3 having extra charges of 250 and 250 and 275 kg TNT, respectively. The payloads considered for the two storey-three span frames (3F) included 50, 75, 100, 150, 200, 250, 300, 500, 750, 1000, 1100, 1250, 1350 and 1500 kg TNT with 3F2 and 3F3 having extra charges of 1600, 1700 and 1800 kg TNT, all applied at a distance of 30m. For the two storey-five span frames (5F) the payloads included 150, 300, 400, 500, 700, 1000, 1500, 2000, 2500, 3000, 3500, 4000, 4500, 5000 and 5250 kg TNT exploding at a distance of 50m from the frames.

ii) For each frame and for each explosion payload, the calculated blast pressure time histories were applied to their respective faces (near, far and roof) of the frame and a transient dynamic analysis was performed on the frame considering both an elastic linear and an elasto-plastic non-linear response to determine the member stresses, base shear and drift time histories for each type of response. The time step considered for the transient dynamic analysis was 0.05 ms. Therefore, for example, the duration of the time history given in Fig. 5a for the U frame is 27.3 ms, giving 546 time steps for the transient analysis of this frame. Typical time history results, in the form of time history of the displacement at the roof level (drift) of frame U_1 are presented in Fig. 9. As can be observed, in the linear elastic case, the displacement varies sinusoidaly, indicating an elastic free vibration of the frame after the blast. However, in the non-linear model the blast causes a permanent drift and the displacement oscillates around the permanent drift. The time history of bending moment for the bottom and top of the columns of U_1 are also shown in Figs. 10 and 11, respectively. The variations in the bending moments shown in Fig. 10a or 10b follow a general,

free vibration trend. However, some secondary effects can be seen superimposed on this general trend. In this figure, the secondary effects are shown up to 0.1 sec., but, for clarity of the general trend, they are eliminated from the figures after that time.

iii) The maximum base shear and the maximum drift obtained from the linear and non-linear dynamic blast analyses of each frame under each payload are then extracted and used to draw the base shear-drift curve for that frame. The base shear-drift curves thus obtained from the linear and non-linear analyses for frames U_1, U_2 and U_3 are shown separately in Fig. 12. Using these diagrams and with reference to Fig. 8, the parameters F_e, F_y and R_μ are calculated and are presented in Table 3.

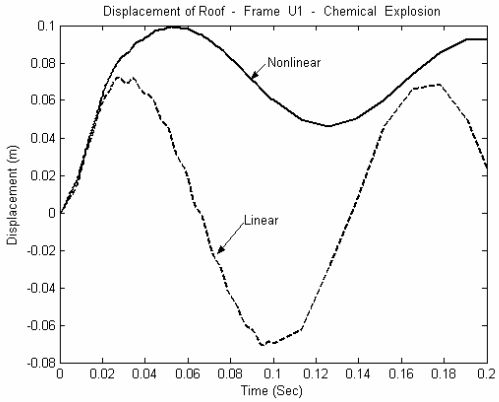

Fig. 9. Time history of roof displacement for U_1 frame

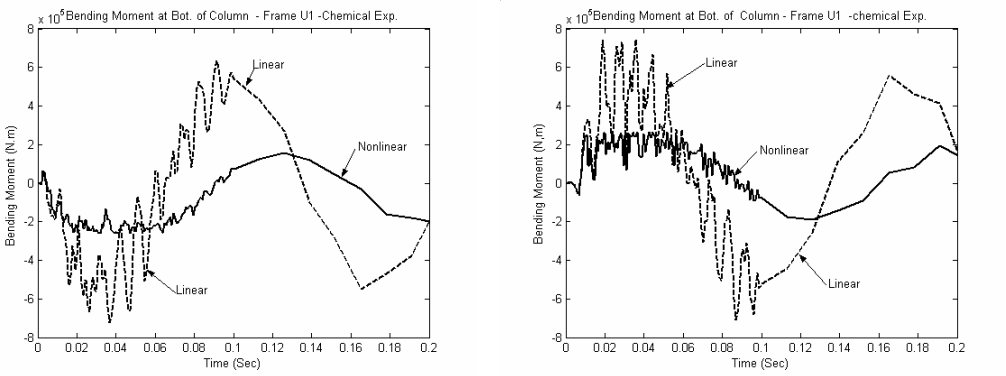

a) b)

Fig. 10. Time history of bending moment for bottom of the columns of U_1;
a) near side, b) far side

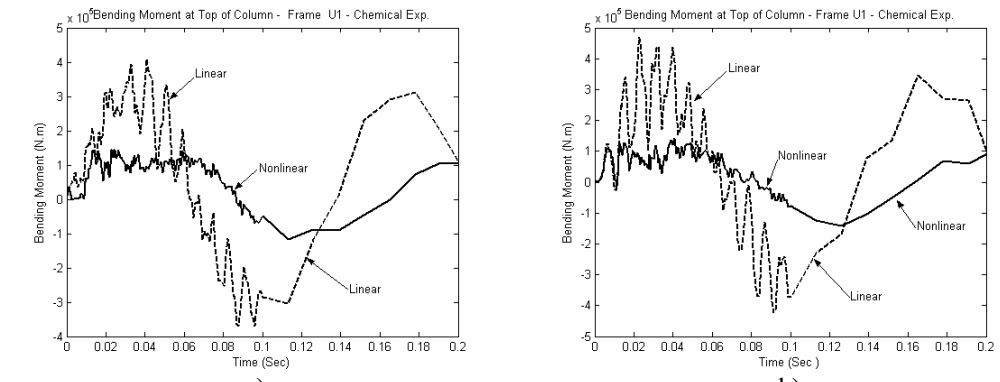

a) b)

Fig. 11. Time history of bending moment for top of the columns of U_1,
a) near side, b) far side

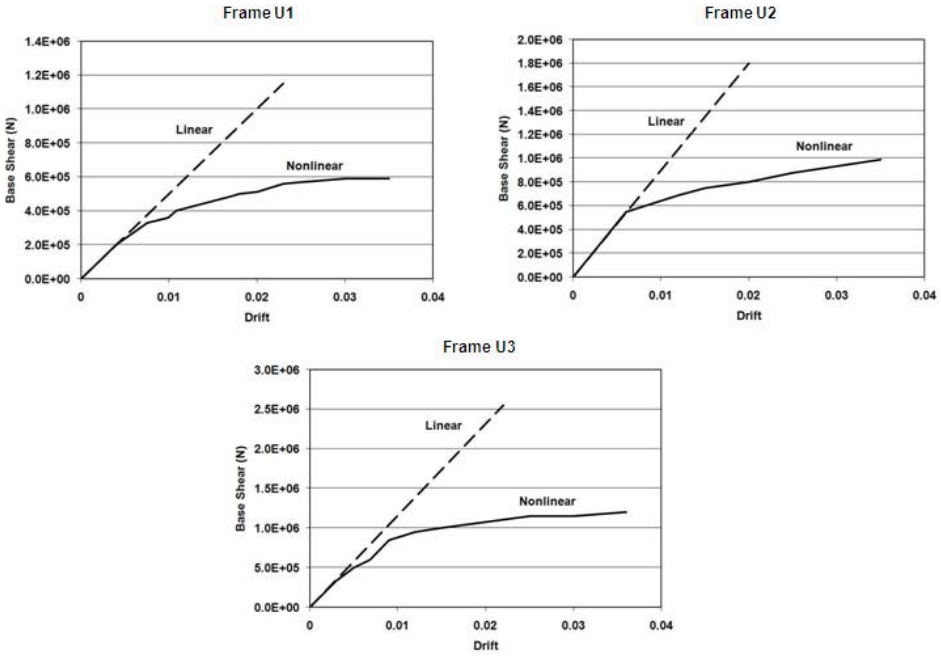

Fig. 12. Drift-base shear diagrams for one span-one storey (U) frames

Table 3. The amount of F_e, F_y and R_μ for one span-one storey frames

	U_1	U_2	U_3
F_e (kN)	943	1708	1955
F_y (kN)	554	745	829
$R_\mu = F_e/F_y$	1.70	2.29	2.36

Similarly, linear and non-linear blast analyses for two-storey frames 3F and 5F were carried out. The base shear-drift curves for the 3-span frames ($3F_1$, $3F_2$ and $3F_3$) and the 5-storey frames ($5F_1$, $5F_2$ and $5F_3$) are shown in Fig. 13 and Fig. 14, respectively. Also, in Table 4, the parameters F_e, F_y and R_μ, deduced from the results of analyses on the 3-span and 5-span frames are presented. Figures 13 and 14 and Tables 4 demonstrate that in all cases as the ductility ratio of a frame increases, the ductility reduction factor also increases. This indicates the improvement of the structural behavior with increased ductility.

Table 4. F_e, F_y and R_μ for three and five span-two storey frames

	3F1	3F2	3F3	5F1	5F2	5F3
F_e	1547	1676	2897	1720	1935	3870
F_y	474	502	698	646.8	683.5	905
F_e/F_y	3.26	3.34	4.14	2.66	2.84	4.27

5. A DISCUSSION ON THE RESULTS

To compare the results of different frames having similar ductility ratios, the drift-base shear curves from the non-linear analyses of the frames are presented in Fig. 15. Frames U_2 ($\mu = 3.4$), $3F_1$ ($\mu = 3.3$) and $5F_1$ ($\mu = 3.3$) are compared in Fig. 15a, and frames U_3 ($\mu = 3.8$), $3F_2$ ($\mu = 3.7$) and $5F_2$ ($\mu = 3.8$) are compared in Fig. 15b.

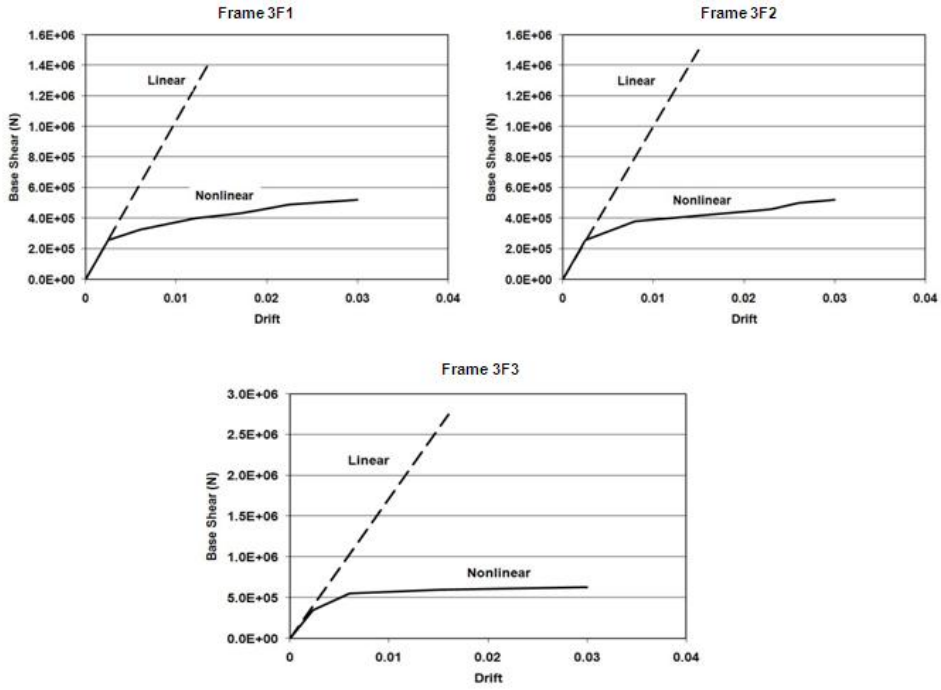

Fig. 13. Drift-base shear diagrams for three span-two storey frames

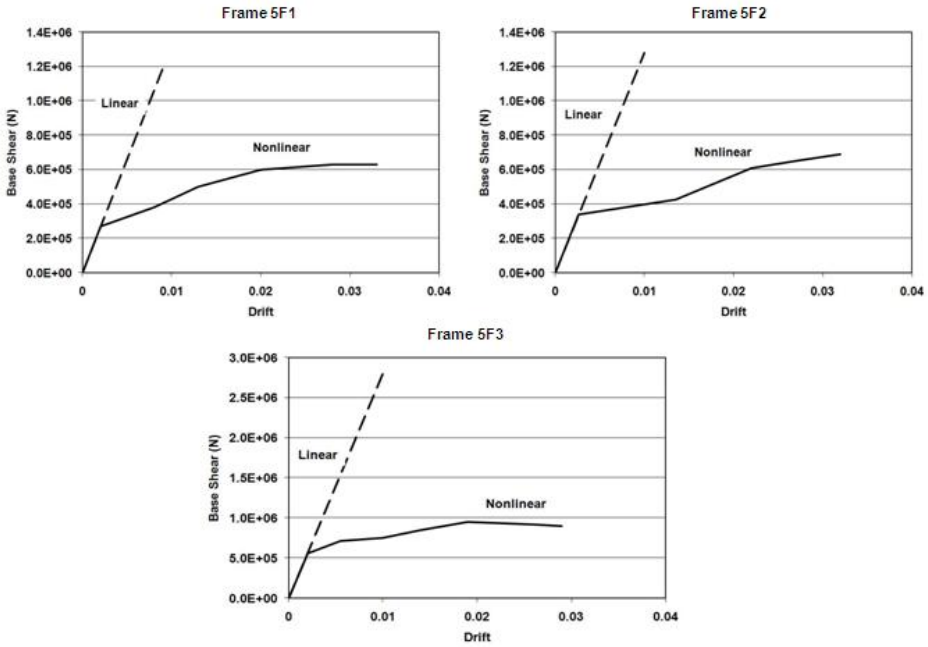

Fig. 14. Drift-base shear diagrams for five span-two storey frames

Considering the differences in the number of the spans, and the cross-section of the members of the frames, a better comparison can be achieved if the base shear-drift curves of Fig. 15 are scaled in relation to their F_y. The scaled base shear-drift are shown in Fig. 16. Fig. 16 demonstrates that, in spite of the differences in the number of spans, number of storeys, the height of frames and physical specification of the members, the structures with similar ductility ratios have similar scaled base shears. The exception being the single storey frame U3 which appears to follow a different trend. However, the importance of ductility in reducing the blast loading on the frames appears to be true for all the frames. To further

compare the effects of ductility ratio μ on the ductility reduction factor R_μ, the results for all nine frames are presented in Fig. 17. It can be seen that for $\mu \leq 3.3$ and $\mu \geq 3.8$ the R_μ dependence on μ is very high. On the other hand, for ductility ratios between 3.3 and 3.8, the changes in R_μ with increasing μ appear to be of a lower order when compared with ductility ratios outside this range. However, Fig. 17 indicates that for all the frames investigated and under all circumstances, the ductility reduction factor R_μ increases with increasing μ.

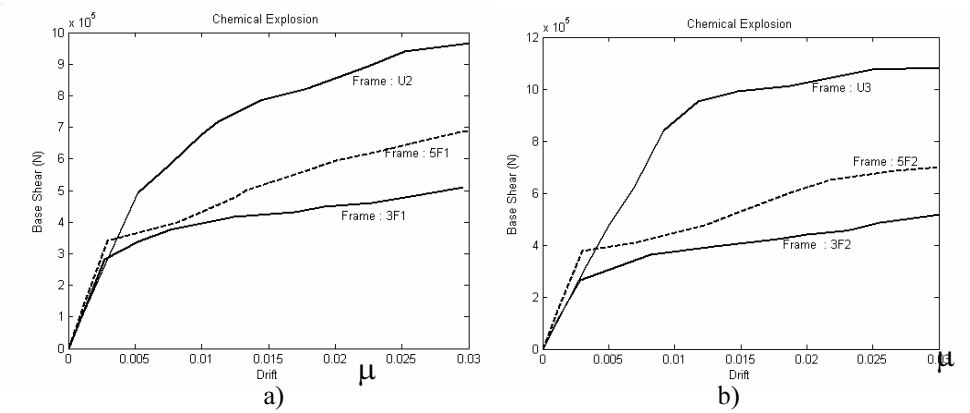

a) b)

Fig. 15. Comparison between base shear-drift diagrams for frames having,
a) $\mu = 3.3 - 3.4$ b) $\mu = 3.7 - 3.8$

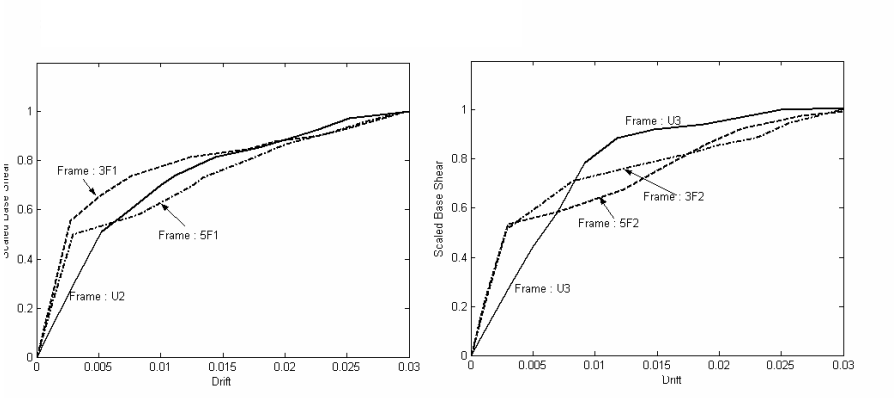

a) b)

Fig. 16. Comparison of scaled base shear-drift diagrams for frames having,
a) $\mu = 3.3 - 3.4$ b) $\mu = 3.7 - 3.8$

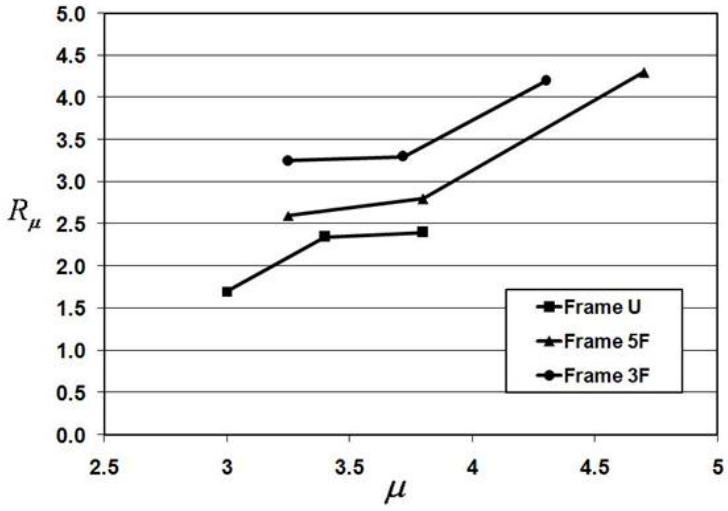

Fig. 17. Ductility reduction factor versus ductility ratio

At this stage it would be prudent to compare the ductility effects under blast loading with that of the earthquake loading. The effect of ductility on reducing the earthquake loading has been investigated by a number of investigators. Newmark and Hall [23] studied the linear and non-linear spectrums of a number of earthquakes to determine the ductility reduction factor, R_μ, and presented it as a function of the ductility ratio, μ, and the fundamental period of vibration of the structure. Lai and Biggs [24] also used the non-linear spectrums of 20 synthetic earthquakes and presented the ductility reduction factor as a logarithmic function of μ. Riddell and Newmark [25] used statistical studies of non-linear spectrums of elasto-plastic systems to derive at a relationship for R_μ. In another study, Riddell et al. [26] used the time histories of four sets of earthquakes to derive a bilinear relation for determination of R_μ. Nassar and Krawinkler [27] presented another relationship for R_μ as a function of μ and T. They used time histories of 15 earthquakes recorded on hard rock and alluvium in the west of the United States. Finally, Miranda and Bertero [28] used the time histories of 124 earthquakes recorded on different types of soil and presented R_μ for three different soil types.

Using the relationships given by the above investigators, the earthquake ductility reduction factors for the frames U, 3F and 5F are determined and compared with the ductility reduction factor obtained from the blast loading of the same frames in Table 5. Also, in Fig. 18, different values of R_μ obtained from earthquake loading and blast loading for frames U1, U2 and U3 are presented. It is evident that the values obtained using the relationship presented by Lai and Biggs differ considerably with those obtained from the rest of the earthquake-related ductility reduction factors. Also, the values deduced from the relationships given by Newmark and Hall and Riddell and Newmark show that for the one-storey frames, U, depending on the ductility ratio, the ductility reduction factor may be inversely proportional to μ [23, 25]. This is not shown by other investigators and is in contrast with the results obtained from the present study for blast loading. On the other hand, the results obtained from the Riddell et al., Nassar and Krawinkler and Miranda and Bertero relationships conform well, for all the frames [26-28]. Therefore, the average of the results from the latter three references are considered for the earthquake-related R_μ for frame U and the average R_μ from all the investigators (except Lai and Biggs) is used for frames 3F and 5F. The values representing the average earthquake-related R_μ are compared with the blast-related R_μ in Fig. 18. The results shown in Fig. 18 indicate that for both the earthquake and blast loading, and for all frames, R_μ increases with increasing μ. Also, although the importance of ductility in reducing the blast loading is evident from these results, it can clearly be seen that ductility has a more important role in earthquake loading compared to blast loading of the structures.

Table 5. Ductility reduction factor in earthquake and blast loading

Frame	U_1	U_2	U_3	3F1	3F2	3F3	5F1	5F2	5F3
T (sec)	.537	.414	.356	.884	.871	.731	1.00	.959	.741
μ	3	3.4	3.8	3.3	3.7	4.3	3.3	3.8	4.7
Blast loading	1.70	2.29	2.36	3.26	3.34	4.14	2.66	2.84	4.27
Newmark & Hall [23]	2.9	2.4	2.5	3.3	3.7	4.3	3.3	3.8	4.7
Lai & Biggs [24]	2.0	2.1	2.2	2.6	2.7	3.1	2.65	3.0	3.2
Riddell & Newmark [25]	2.8	2.4	2.5	3.3	3.6	3.95	3.3	3.65	4.15
Riddell &Hidalgo &Cruz [26]	3.2	3.4	3.8	3.3	3.7	4.3	3.3	3.8	4.7
Nassar & Krawinkler [27]	2.95	3.2	3.45	3.55	4.05	4.65	3.6	4.2	5.15
Miranda & Bertero; (Rock) [28]	2.7	2.8	3.0	3.5	3.9	4.2	3.7	4.2	4.5
Miranda & Bertero; (Alluvium)	3.0	3.0	3.25	4.0	4.5	4.9	4.1	4.7	5.3

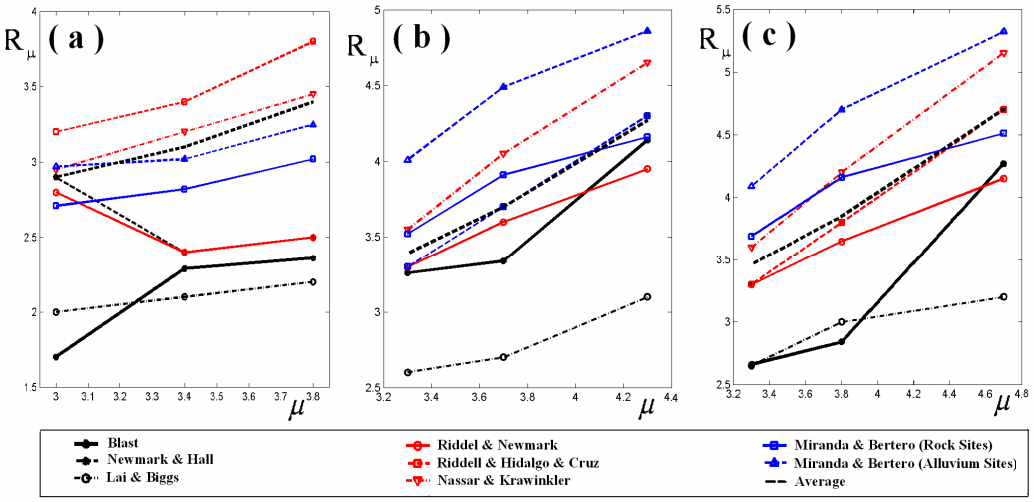

Fig. 18. Comparison between ductility reduction factor in earthquake and blast loading

6. CONCLUSION

In this article the behaviour of nine steel frames, having different geometrical configurations, dimensional specifications and ductility ratios, subjected to blast loading were investigated. The results of these investigations lead us to the following conclusions;

1. Similar to earthquake loading, in blast loading ductility ratio is the dominant parameter when determining the ductility reduction factor.
2. Similar to earthquake loading, the ductility reduction factor under blast loading increases with increasing ductility ratio, irrespective of the period of vibration of the system.
3. It seems that the ductility ratio has a more profound effect on reducing the earthquake loading compared to blast loading. However, the importance of ductility of the structure in reducing the effects of blast loading on the structure is also clearly shown. The ductility reduction factor R_μ was evaluated as between 2 to 4 for ductility ratios μ from 3 to 4.7 for different frames, indicating the importance of this parameter when designing for blast loading.

REFERENCES

1. Smith, P. D. & Heatherington, J. G. (1994). *Blast and ballistic loading of structures*. Butterworth- Heinemann Ltd- UK.
2. Smilowitz, R. (2005). *Analytical tools for progressvie collapse analysis*. Weidlinger Associates.
3. Thabet, A. & Haldane, D. (2000). Three-dimensional simulation of nonlinear response of reinforced concrete members subjected to impact loading. *ACI Structural Journal*, Vol. 97, No. 5, pp. 689-702.
4. Mendis, P. & Ngo, T. (2003). Vulnerability assessment of concrete tall buildings subjected to extreme loading conditions. *CIB_ CTBUH, International Conference on Tall Buildings,* Malaysia.
5. Hinman, E. (2003). Retrofitting buildings to resist explosive attack. *Presentation to the Existing Bulding Committee of the SEAONC*.
6. Khaloo, A. R. & Tariverdilu Asl, S. (2001). Ductility evaluation of confined high-strength concrete flexural members. *Iranian Journal of Science and Technology, Transaction B, Engineering*, Vol. 25, No. B1, 129-131.
7. Son, J., Astaneh- Asl, A., Runter, A. M. (2005). Performance of bridges subjected to blast load. *6th-Japanese-German Bridge Symposium*, Munich.
8. Runter, M., Astaneh-Asl, A. & Son, J. (2005). Protection of bridge piers against blast. *6th - Japanese- German Bridge Symposium*, Munich, Germany.

9. Luccioni, B. M. & Luege, M. (2006). Concrete pavement slab under blast loads. *International Journal of Impact Engineering*, Vol.32, pp.1248-1266.
10. Miyamoto, A. & Nakamura, H. (2001). Visualization of impact failure behavior for RC slabs. P*roceeding of 3rd International Conference on Concrete under Severe Conditions*, UBC.
11. Lan, S., Lok, T. S. & Heng, L. (2005). Composite structural panels subjected to explosive loading. *Construction and Bulding Materials*, Vol. 19, pp. 387-395.
12. Librescu, L. S., Oh, Y. & Hohe, J. (2004). Linear and non-linear dynamic response of sandwich panels to blast loading. *Composites, Part B*, Vol. 35, pp. 673-683.
13. Louca, L. A. & Boh, J. W. (2004). Analysis and design of profiled blast walls. *Prepared by Imperial College London for the Health and Safety Executive*. Department of Civil and Environmental Engineering, South Kensington, London, SW7-2AZ.
14. Magnusson, J. & Hallgre, M. (2004). Reinforced high strength concrete beam subject to air blast loading. *Structures and Materials*, VIS, *Structures under Shock and Impact* VIII, pp. 53-62.
15. Newmark, N. M. & Hall, W. J. (1982). *Earthquake spectra and design.* Berkeley, CA: Earthquake Engineering Research Institute.
16. ANSYS, *Release 11.0 Documentation for ANSYS.*, Available://www.kxcad.net/ansys/.
17. Standard No. 2800-05 (2005). *Iranian code of practice for seismic resistant design of buildings.* Third ed., Building and Housing Research Center, BHRC Publication, Tehran.
18. Kinney, G. F. & Graham, K. J. (1985). *Explosive shocks in air*. *2nd Ed*., Berlin: Springer.
19. TM5, (1990). *Design of structures to resist the effects of accidental explosions*. S Department of Army- TM5-1300
20. Izadifard, R. A. (2008). Ductility effects on the behaviour of steel structures under blast loading. *Doctoral Thesis, Department of Civil Engineering*, Shiraz University, IRAN.
21. Bangash, M. Y. H. & Bangash, T. (2006). *Explosion- resistant buildings.* Springer Pub.
22. Izadifard, R. A. & Maheri, M. R. (2008). Application of DBD method to assess the level of structural damage due to blast loads. *Journal of Mechanical Science And Technology* (in press).
23. Newmark, N. M. & Hall, W. J. (1973). Seismic design criteria for nuclear reactor facilities. *Report No. 46, Building Practices for Disaster Mitigation,* National Bureau Department of Commerce, pp.209-236.
24. Lai, S. P. & Biggs, J. M. (1980). Inelastic response spectra for aseismic building design. *J. Struct. Div., ASCE,* Vol. 106, No. ST6, pp. 1295-1310.
25. Riddell, R. & Newmark, N. M. (1979). Statistical analysis of the response of nonlinear systems subjected to earthquakes. *Structural Research Series No. 468,* Dept. of Civ. Eng., University of Illinois, Urbana.
26. Riddell, R., Hidalgo, P. & Cruz, E. (1991). Response modification factors for earthquake resistant design of short period structures. *Earthquake Spectra,* Vol. 5, No. 3, pp.571-590.
27. Nassar, A. A. & Krawinkler, H. (1991). Seismic demands for SDOF and MDOF systems. *Report No. 95, The John A. Blume Earthquake Engineering Center,* Stanford University, Stanford, California.
28. Miranda, E. & Bertero, V. (1994). Evaluation of strength reduction factors for earthquake-resistant design. *Earthquake Spectra,* Vol.10, No.2, pp.357-379.